

**Interference of Higgs diphoton signal and background in production with a jet at the LHC**

Stephen P. Martin

*Department of Physics, Northern Illinois University, DeKalb, Illinois 60115, USA  
and Fermi National Accelerator Laboratory, P.O. Box 500, Batavia, Illinois 60510, USA*  
(Received 26 March 2013; published 8 July 2013)

The Higgs mass determination from diphoton events at the LHC can be affected by interference between the Higgs resonant and continuum background amplitudes with the same initial and final states. For the leading order gluon fusion process, this shift was previously found to exceed 100 MeV, with some dependence on the diphoton mass resolution and the methods used to extract and fit the peak from data. In this paper, I consider the mass shift for the process  $pp \rightarrow j\gamma\gamma$  that includes an additional central jet in the final state. For cuts on the transverse momentum of the jet of 25 GeV or more, the diphoton Higgs peak mass shift due to interference is found to be very small, due in part to less interference for the gluon-gluon initiated subprocess, and in part to a cancellation between it and the quark-gluon initiated subprocess.

DOI: [10.1103/PhysRevD.88.013004](https://doi.org/10.1103/PhysRevD.88.013004)

PACS numbers: 14.80.Bn

**I. INTRODUCTION**

The ATLAS and CMS detector collaborations at the LHC have recently established [1–4] the existence of a resonance whose properties are consistent with those of the minimal Standard Model Higgs scalar boson,  $H$ . The properties of this resonance are now the subject of detailed theoretical and experimental investigations to establish its quantum numbers, couplings, and mass. Given the absence of direct or indirect indications for a nonminimal electroweak symmetry breaking mechanism, it will be assumed here that the resonance is indeed  $H$ .

The mass determination of  $H$  is driven primarily by the invariant mass peaks in the  $\gamma\gamma$  and  $ZZ^* \rightarrow \ell^+\ell^-\ell'^+\ell'^-$  channels. The production of  $H$  is mostly due to  $gg \rightarrow H$  [5], for which a great effort has been made to include higher order effects, notably up to next-to-next-to-leading order in QCD [6–19], next-to-leading order (NLO) in electroweak couplings [20–22], and next-to-next-to-leading logs in soft gluon resummation [23–25]. These contributions are reviewed in [26–29]. However, because the mass measurement comes from invariant mass distributions, for the most part it does not depend directly on the details of the Higgs production, including the significant remaining uncertainty on the total rate and the presence of additional hadrons. The best experimental values for the mass combining the  $\gamma\gamma$  and  $ZZ^*$  channels at this writing are

$$M_H = 125.5 \pm 0.2_{-0.6}^{+0.5} \text{ GeV} \quad (\text{ATLAS [3]}), \quad (1.1)$$

$$M_H = 125.8 \pm 0.4 \pm 0.4 \text{ GeV} \quad (\text{CMS [4]}). \quad (1.2)$$

In each case, the first uncertainty is statistical and the second is systematic. In the future, one may hope to achieve much more precise values, given more statistics and reduced systematic uncertainties. Even now, it is worth accounting for effects on the mass determination of order 0.1 GeV, since this is the last digit being reported by the experimental collaborations.

One of the issues that may need to be confronted in a precision determination of  $M_H$  is the effect of the interference between resonant Higgs production amplitudes and the continuum (non-Higgs-mediated) amplitudes with the same initial and final states. The interference effect can produce small shifts in the invariant mass distributions, which are in principle observable because they differ for different parton-level processes. In particular, for the diphoton channel the interference effect is not completely negligible because of the relatively large continuum amplitude (one-loop order) compared to the Higgs-mediated amplitude (which is two-loop order; there are no renormalizable couplings of the neutral  $H$  to  $\gamma\gamma$  or to  $gg$ ). In Ref. [30], it was shown that in the leading order parton-level process  $gg \rightarrow \gamma\gamma$ , interference effects can shift the position of the Higgs diphoton invariant mass peak lower by over 100 MeV compared to where it would be ignoring the interference. Since the latter corresponds to what should be obtained in the  $ZZ$  and vector boson fusion channels, which will not have such a significant interference effect, this shift is observable. The magnitude of the shift will depend on the method used to fit to the diphoton peak and will also be greatly affected by higher order corrections and by cuts and kinematic-dependent detector efficiencies.

In general, the diphoton mass line shape in proton-proton collisions can be written in terms of the invariant mass of the diphoton pair,  $\sqrt{h} \equiv M_{\gamma\gamma}$ , as the sum of a continuum plus a Breit-Wigner peak multiplied by functions that are approximately symmetric and antisymmetric about the Higgs pole mass:

$$\frac{d\sigma_{pp \rightarrow \gamma\gamma+X}}{d(\sqrt{h})} = C(h) + \frac{1}{D(h)} [P(h) + (h - M_H^2)I(h)]. \quad (1.3)$$

Here,  $C(h)$ ,  $P(h)$ , and  $I(h)$  are smooth functions of  $h$  near the resonance, and

$$D(h) \equiv (h - M_H^2)^2 + M_H^2 \Gamma_H^2, \quad (1.4)$$

where  $M_H$  is the Breit-Wigner mass of the Higgs from the renormalized propagator, and  $\Gamma_H$  is the Higgs total decay width. The function  $C(h)$  arises from the continuum involving Feynman diagrams that do not include the Higgs boson. It falls smoothly with  $h$  and is determined by the experimental collaborations by sideband analyses, fitting to data away from the diphoton peak. Because this is most accurately determined experimentally, it will not be considered as an object of theoretical computation here. The function  $P(h)$  arises mostly from the pure Higgs resonance diagrams squared, with a small contribution from the interference. Almost all previous studies of the Higgs diphoton signal have relied on the narrow width approximation in which  $1/D(h) \approx \pi \delta(h - M_H^2)/M_H \Gamma_H$ , and one evaluates  $H + X$  production separately from the on-shell decays of  $H$ , including the diphoton decay [31–36]. In that approximation, the function  $I(h)$  does not appear. In general, the function  $I(h)$  arises only from the interference terms between Higgs resonant and continuum amplitudes. Its importance is that it gives rise to a shift in the diphoton mass distribution peak away from  $M_H$ , since the corresponding contribution to the cross section is odd in  $\sqrt{h} - M_H$ . The sign of the shift in the diphoton mass peak, compared to its position if interference were neglected, is the same as the sign of  $I(h)$ . The magnitude of the mass shift depends on the relative sizes of  $I(h)$  and  $P(h)$  with kinematic cuts (to be evaluated numerically below) and detector effects including the diphoton mass resolution.

In contrast, the effect of interference on the total cross section is very small at leading order [37,38], while at next-to-leading order there is a reduction of a few percent [38] due to the imaginary part of the two-loop continuum amplitude  $gg \rightarrow \gamma\gamma$  from light quark loops [39]. Other studies of the effects of interference between signal and background in Higgs production in different contexts can be found in Refs. [40–44].

The leading order shift in the Higgs mass peak due to interference should be investigated with a full NLO calculation, at least. As a precursor to this, in the present paper I will investigate the interference between signal and background for processes contributing to diphoton production with an additional central jet requirement imposed on the final state,  $pp \rightarrow j\gamma\gamma$ . The parton-level processes  $Qg \rightarrow Q\gamma\gamma$ ,  $\bar{Q}g \rightarrow \bar{Q}\gamma\gamma$ , and  $Q\bar{Q} \rightarrow g\gamma\gamma$  are suppressed by relatively small quark parton distribution functions, but this is counteracted in part by the fact that the continuum amplitudes are tree level, providing for a stronger interference with the Higgs resonant amplitudes, compared to the noninterference contributions. These processes have recently been investigated in [45], where it is found that the diphoton mass distribution shift is in the opposite direction to the leading order  $gg \rightarrow \gamma\gamma$  shift. I find agreement with their result, and in the present paper I will

include also the  $gg \rightarrow g\gamma\gamma$  process, which has a mass shift with the same sign as the shift from  $gg \rightarrow \gamma\gamma$ .

Previous investigations [9,46–49] of the  $pp \rightarrow jH$  signal for the LHC have considered a cut on  $p_T^j$  of 30 GeV or higher. In the present paper this cut will be varied to both much larger and much smaller values. In the limit that the  $p_T^j$  cut on the final-state jet is taken to be very small (certainly for less than 15 GeV or so), the results are clearly unphysical, as the real emission of a soft jet is subject to infrared log divergences that should be regularized and canceled against those coming from virtual corrections to the leading-order process  $gg \rightarrow \gamma\gamma$  in a full NLO calculation. Nevertheless, I will include below the experimentally unrealistic case of very low  $p_T^j$  cuts even below 1 GeV, since this provides a check; the result for the mass shift due to interference in this case approaches that for the leading-order process, as the calculated production is dominated by the leading order subdiagrams  $gg \rightarrow \gamma\gamma$  with a soft gluon emission attached to them.

The rest of this paper is organized as follows. In Sec. II, the situation for the leading order process without an extra jet is reviewed, following Ref. [30], and including numerical results for the same cuts on the photons as will be imposed later on in the process with an additional jet. Section III provides analytical formulas for the pure Higgs and interference contributions to  $pp \rightarrow j\gamma\gamma$ . Numerical results are then discussed in Sec. IV. Section V contains some summarizing remarks.

## II. HIGGS INTERFERENCE IN $pp \rightarrow \gamma\gamma$

The leading order diphoton production cross section relevant to Higgs production and interference can be written as

$$\begin{aligned} \frac{d\sigma_{pp \rightarrow \gamma\gamma}}{d(\sqrt{h})} &= \frac{1}{128\pi\sqrt{h}D(h)} \\ &\times \int_{\ln\sqrt{\tau}}^{-\ln\sqrt{\tau}} \frac{dy}{s} g(\sqrt{\tau}e^y, \mu_F^2) g(\sqrt{\tau}e^{-y}, \mu_F^2) \\ &\times \int_{-1}^1 dz \Theta(h, y, z) N(h, z), \end{aligned} \quad (2.1)$$

where  $\tau = h/s$ , with  $\sqrt{s}$  the fixed total energy of the  $pp$  collisions at the LHC,  $g(x, \mu_F^2)$  is the gluon parton distribution function,  $y$  is the longitudinal rapidity of the partonic center-of-momentum frame,  $z$  is the cosine of the photon scattering angle with respect to the beam axis, and  $\Theta(h, y, z)$  represents the effects of kinematic cuts. The resonant and interference contributions to  $N(h, z)$  are  $N_H + N_{\text{int,Re}} + N_{\text{int,Im}}$ , with

$$N_H = h^2 |C_g C_\gamma|^2 / 4, \quad (2.2)$$

$$N_{\text{int,Re}} = -(h - M_H^2) h \text{Re}[C_g C_\gamma A_{gg\gamma\gamma}^*], \quad (2.3)$$

$$N_{\text{int,Im}} = -M_H \Gamma_H h \text{Im}[C_g C_\gamma A_{gg\gamma\gamma}^*]. \quad (2.4)$$

Here, the effective Higgs coupling to gluons, in the limit of a very heavy top quark and other quarks massless, is parametrized by

$$C_g = \frac{\alpha_S}{3\pi v}, \quad (2.5)$$

using a normalization where  $v \approx 246$  GeV is the Higgs expectation value. This  $M_t \rightarrow \infty$  effective theory for the Higgs interactions with gluons (both  $Hgg$  and  $Hggg$ ) is a good approximation [6,7,32,50] for the realistic case (with  $M_H \sim 125$  GeV and  $M_t = 173$  GeV) for transverse momenta less than  $M_t$  and will be used throughout this paper. The Higgs interaction with photons is instead treated using the complete one-loop expression:

$$C_\gamma = -\frac{\alpha h}{4\pi v} \left[ F_1(4m_W^2/h) + \sum_{f=i,b,c,\tau} N_c^f e_f^2 F_{1/2}(4m_f^2/h) \right], \quad (2.6)$$

where  $N_c^f = 3$  (1) for  $f =$  quarks (leptons) with electric charge  $e_f$  and mass  $m_f$ , and

$$F_1(x) = 2 + 3x[1 + (2-x)f(x)], \quad (2.7)$$

$$F_{1/2}(x) = -2x[1 + (1-x)f(x)], \quad (2.8)$$

$$f(x) = \begin{cases} \left[ \arcsin(\sqrt{1/x}) \right]^2, & x \geq 1 \quad (\text{for } t, W), \\ -\frac{1}{4} \left[ \ln\left(\frac{1+\sqrt{1-x}}{1-\sqrt{1-x}}\right) - i\pi \right]^2, & x \leq 1 \quad (\text{for } b, c, \tau). \end{cases} \quad (2.9)$$

(The effective Higgs couplings used in Ref. [30] are related to these definitions by  $A_{\gamma\gamma H} = C_\gamma$  and  $A_{ggH} = hC_g/2$ , and the variable  $\hat{s}$  there is the same as  $h$  here.) For the continuum amplitude contribution [51–53], the heavy top and massless  $u$ ,  $d$ ,  $c$ ,  $s$ ,  $b$  approximation is also used here, leading to

$$A_{gg\gamma\gamma} = \frac{22}{9} \alpha_S \alpha \left\{ z \ln\left(\frac{1+z}{1-z}\right) - \frac{1+z^2}{4} \left[ \ln^2\left(\frac{1+z}{1-z}\right) + \pi^2 \right] \right\}. \quad (2.10)$$

The numerical effect of including a finite top mass and nonzero bottom mass is not very large for the interference effect as it applies to the diphoton mass shift.

For  $pp \rightarrow \gamma\gamma$ , the cuts on the transverse momenta and pseudorapidity of the photons are

$$p_{T\gamma} > p_{T\gamma}^{\text{cut}} = 40 \text{ GeV}, \quad (2.11)$$

$$|\eta_\gamma| < \eta_\gamma^{\text{cut}} = 2.5. \quad (2.12)$$

These cuts are implemented in the numerical integration of this section (with no extra jet) simply by imposing the restrictions that  $|y| < \eta_\gamma^{\text{cut}}$  and that  $|z|$  is less than both

$\sqrt{1 - 4(p_{T\gamma}^{\text{cut}})^2/h}$  and  $\tanh(\eta_\gamma^{\text{cut}} - |y|)$ . The results below therefore differ from Ref. [30], where these cuts on the photons were mentioned but not directly applied. The impact of this is to reduce the mass shift due to the interference somewhat.

For purposes of illustration, I take  $M_H = 125$  GeV and  $\Gamma_G = 4.2$  MeV. The parameter  $C_\gamma$  is evaluated using  $m_t = 168.2$  GeV,  $m_b = 2.78$  GeV,  $m_c = 0.72$  GeV,  $m_\tau = 1.744$  GeV, and  $\alpha = 1/127.5$ . Also, to facilitate comparison with an eventual NLO calculation, I have used MSTW 2008 NLO [54] parton distribution functions with factorization scale  $\mu_F = M_H$  and evaluated the corresponding strong coupling at the same renormalization scale  $\mu_R = M_H$ ; explicitly this is  $\alpha_S(M_H) = 0.114629$ . The unsmeared diphoton line shape is shown in Fig. 1. For  $\sqrt{h}$  very close to  $M_H$ , the line shapes are nearly indistinguishable, but for  $|\sqrt{h} - M_H| \gtrsim 50$  MeV, the magnitude of the interference term is much larger than the pure resonance contribution, due to the long tails of the square root of the Breit-Wigner line shape. The effect of the interference is to produce slightly more events below  $M_H$  than above  $M_H$ , because the function  $I(h)$  in Eq. (1.3) is negative near  $\sqrt{h} = M_H$ .

The effects of detector resolution are complicated, depending on the location and type of interaction of photons in the detector. For simplicity, I assume a Gaussian invariant mass resolution, with mass resolution widths  $\sigma_{\text{MR}}$ . For a typical case  $\sigma_{\text{MR}} = 1.7$  GeV, the diphoton line shape after this Gaussian smearing is shown in Fig. 2. After Gaussian smearing there remains a potentially detectable shift in the diphoton mass distribution.

The magnitude of this shift will depend on the methods used by the experimental collaborations to fit to the line shape, in particular the background. In [30], one measure of this shift was described, but a simpler and better method is to simply do a least-squares fit of the line shapes with and without interference to a Gaussian with the same width  $\sigma_{\text{MR}}$  as was used to model the mass resolution. For the purely resonant contribution without interference included, the peak of the distribution is at  $\sqrt{h} = M_H$  to very high accuracy. In the following, the difference between the centers of the Gaussian fits with and without interference included will be called  $\Delta M_{\gamma\gamma} \equiv M_{\gamma\gamma}^{\text{peak}} - M_H$ . The fit is performed over a range of  $\sqrt{h}$  from 115 to 135 GeV, but the results are not very sensitive to this particular choice. (Even a range 120 to 130 GeV gives nearly the same results, except when  $\sigma_{\text{MR}}$  is larger than about 2.5 GeV.) The magnitude of the shift by this measure is shown in Fig. 3, for varying  $\sigma_{\text{MR}}$  used for both the smearing and the fit. The magnitude of the shift according to this measure actually increases nearly linearly with increasing mass resolution width  $\sigma_{\text{MR}}$ . For a typical average value  $\sigma_{\text{MR}} = 1.7$  GeV, the shift is about  $\Delta M_{\gamma\gamma} = -125$  MeV after cuts; it would be about  $-165$  MeV before the photon  $p_T$  and  $\eta$  cuts. This is because the continuum amplitude has larger

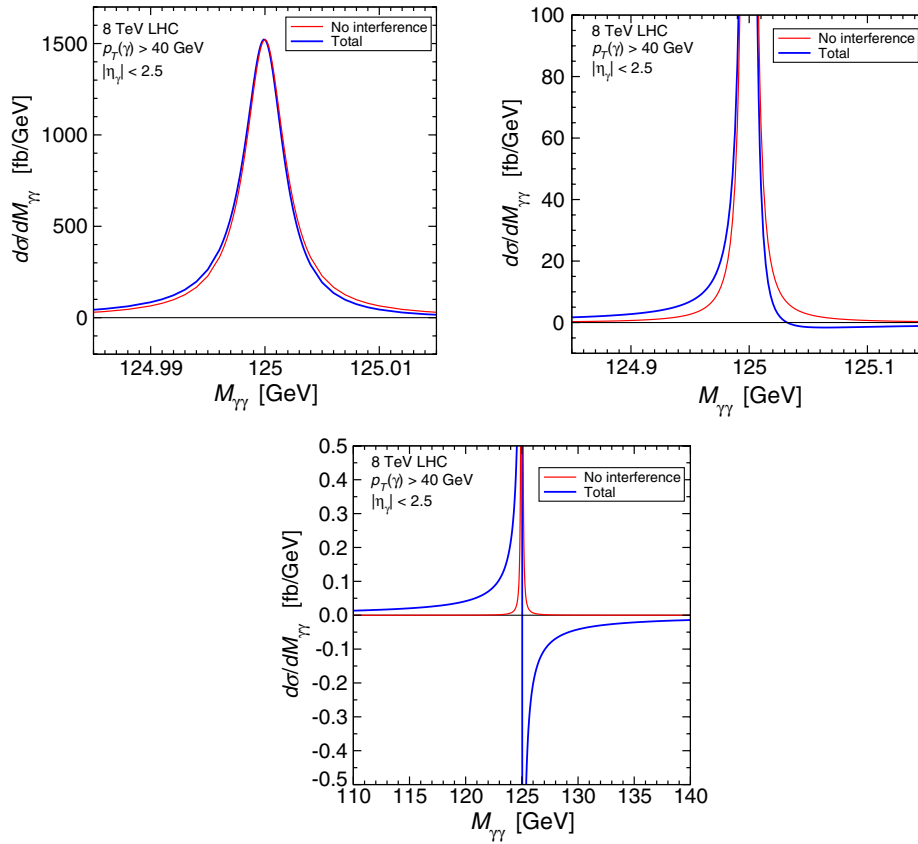


FIG. 1 (color online). The diphoton invariant mass distribution, with and without interference included, before including any experimental resolution effects, computed for  $pp \rightarrow \gamma\gamma$  at leading order as described in Sec. II from the partonic process  $gg \rightarrow \gamma\gamma$ , for 8 TeV  $pp$  collisions at the LHC, with  $p_T > 40$  GeV and  $|\eta| < 2.5$  for the photons. Here  $M_{\gamma\gamma} = \sqrt{\hat{s}}$  is the diphoton mass. The three panels show exactly the same results but with different scales on the axes.

support at small scattering angles ( $z$  near  $\pm 1$ ), due to the logarithms in Eq. (2.10), while the Higgs resonant amplitude is isotropic in the partonic center-of-momentum frame.

The previous results were made with the somewhat arbitrary fixed scale choices  $\mu_R = \mu_F = M_H$ . However,

variations in these scale choices for the strong coupling and the parton distribution functions tend to nearly cancel out of  $\Delta M_{\gamma\gamma}$ , because they enter into the interference term and the pure resonance term in the same way. The choice made here of using the NLO rather than the LO  $\alpha_S(M_H)$  makes the computed total cross sections smaller by about 33%.

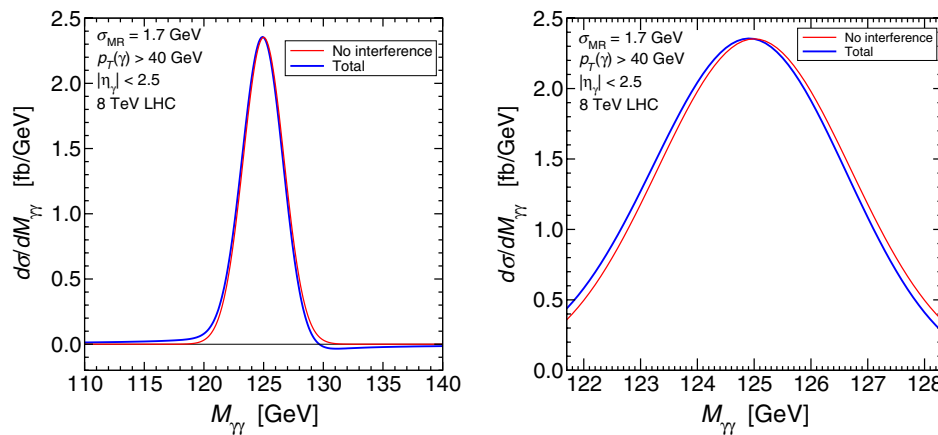


FIG. 2 (color online). The diphoton invariant mass distribution for  $pp \rightarrow \gamma\gamma$  at leading order, with and without interference included, as in Fig. 1, but now including the effects of a Gaussian mass resolution with  $\sigma_{MR} = 1.7$  GeV. The two panels show the same results with different scales on the axes.

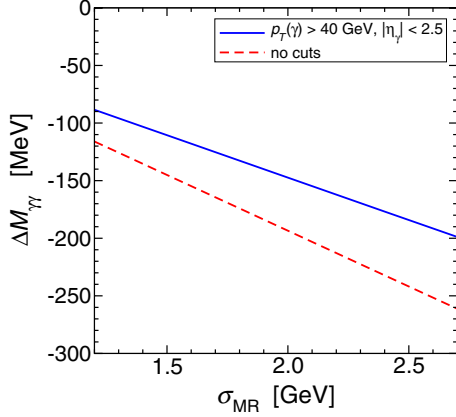


FIG. 3 (color online). The shift in the invariant mass distribution due to the interference effect,  $\Delta M_{\gamma\gamma} \equiv M_{\gamma\gamma}^{\text{peak}} - M_H$ , for  $pp \rightarrow \gamma\gamma$  at leading order, computed by a least-squares fit of the line shape to a Gaussian with the same width  $\sigma_{\text{MR}}$  used to model the mass resolution. The solid line includes cuts  $p_T > 40$  GeV and  $|\eta| < 2.5$  on the photons, and the dashed line is what would be obtained without these cuts.

However, since  $I(h)$  and  $P(h)$  are both proportional to  $\alpha_S^2$ , this dependence very nearly cancels out of the prediction for  $\Delta M_{\gamma\gamma}$ .

### III. HIGGS INTERFERENCE IN $pp \rightarrow j\gamma\gamma$

Now consider the process of Higgs production in association with a jet, in the case where the Higgs decays to two photons. Because the relevant parton level processes  $gg \rightarrow g\gamma\gamma$  and  $Qg \rightarrow Q\gamma\gamma$  and  $\bar{Q}g \rightarrow \bar{Q}\gamma\gamma$  and  $Q\bar{Q} \rightarrow g\gamma\gamma$  have different initial and final states than the  $gg \rightarrow \gamma\gamma$  case studied in the previous section and in [30], it will be no surprise that the interference effect on the mass shift will be different when an extra jet is required by the selection. In fact, the processes involving quarks have continuum amplitudes already at tree level, which provides for a stronger interference with the Higgs resonant amplitudes, compared to the Higgs-only cross sections. However, this effect is mitigated by the smaller quark parton distribution functions for the relevant momentum fractions.

Let us label the initial state partons by 1, 2, and the final state jet parton by 3, and the final state photons by 4, 5. The corresponding momenta and helicities are denoted  $(p_i, \lambda_i)$  for  $i = 1, 2, 3, 4, 5$ . Amplitudes below are evaluated using the spinor helicity formalism following the conventions of Refs. [55,56] for spinor products, and using a convention in which momenta and helicities are always outgoing, even for initial-state particles.

The 4-momenta of the partons are parametrized in terms of the quantities:  $\hat{s}$  (the invariant squared mass of the initial-state partons),  $h$  (the invariant squared mass of the two photons),  $\chi$  (related to the scattering angle of the final-state jet parton), and  $\omega, \phi$  (related to the angles of the

individual photons in the diphoton system rest frame), as follows. In the lab frame,

$$p_1 = -\frac{\sqrt{\hat{s}}}{2}(1, 0, 0, 1), \quad (3.1)$$

$$p_2 = -\frac{\sqrt{\hat{s}}}{2}(1, 0, 0, -1), \quad (3.2)$$

$$p_3 = \frac{\sqrt{\hat{s}}}{2}(1 - h/\hat{s})\left(1, 2\sqrt{\chi(1-\chi)}, 0, 1 - 2\chi\right), \quad (3.3)$$

$$p_H = \frac{\sqrt{\hat{s}}}{2}(1 - h/\hat{s})\left(\frac{\hat{s} + h}{\hat{s} - h}, -2\sqrt{\chi(1-\chi)}, 0, -1 + 2\chi\right), \quad (3.4)$$

where  $H$  denotes the Higgs (or diphoton system), with  $p_H = p_4 + p_5$ . Now  $(p_H, p_4, p_5)$  are related to  $(p'_H, p'_4, p'_5)$  by an appropriate boost, where in the diphoton system rest frame,

$$p'_H = \sqrt{h}(1, 0, 0, 0), \quad (3.5)$$

$$p'_4 = \frac{\sqrt{h}}{2}\left(1, 2\sqrt{\omega(1-\omega)}\cos\phi, 2\sqrt{\omega(1-\omega)}\sin\phi, 1 - 2\omega\right), \quad (3.6)$$

$$p'_5 = \frac{\sqrt{h}}{2}\left(1, -2\sqrt{\omega(1-\omega)}\cos\phi, -2\sqrt{\omega(1-\omega)}\sin\phi, -1 + 2\omega\right). \quad (3.7)$$

(The boost is not written explicitly here, but is determined by the relationship of  $p_H$  and  $p'_H$ .) The ranges for the angular variables are  $0 \leq \chi, \omega \leq 1$  and  $0 \leq \phi < 2\pi$ . Also, define  $s_{ij} = (p_i + p_j)^2$ . Note that

$$\begin{aligned} s_{12} &= (p_1 + p_2)^2 = (p_3 + p_4 + p_5)^2 = \hat{s}, \\ s_{45} &= (p_4 + p_5)^2 = h. \end{aligned} \quad (3.8)$$

We are interested in the diphoton line shape,

$$\begin{aligned} \frac{d\sigma_{pp \rightarrow j\gamma\gamma}}{d(\sqrt{h})} &= \int d\tau \int_{\ln\sqrt{\tau}}^{-\ln\sqrt{\tau}} dy f_1(\sqrt{\tau}e^y, \mu_F^2) \\ &\times f_2(\sqrt{\tau}e^{-y}, \mu_F^2) \frac{d\hat{\sigma}_{12 \rightarrow 345}}{d(\sqrt{h})}, \end{aligned} \quad (3.9)$$

where  $f_{1,2}$  are the distribution functions for the initial-state partons 1 and 2 (which should be summed over), and now  $\tau = \hat{s}/s$ . Including a factor of 1/2 for identical photons, the parton-level differential cross section is

$$\frac{d\hat{\sigma}}{d(\sqrt{h})} = \frac{\sqrt{h}}{512\pi^4\hat{s}}(1 - h/\hat{s}) \int_0^1 d\chi \int_0^1 d\omega \int_0^{2\pi} d\phi \Theta \sum |\mathcal{M}|^2. \quad (3.10)$$

Here  $\mathcal{M}$  is the reduced matrix element for  $12 \rightarrow 345$ , and  $\overline{\sum}$  denotes the average (and sum) over initial (final) state helicities and colors, and  $\Theta(\hat{s}, h, y, \chi, \omega, \phi)$  represents the effects of kinematic cuts, implemented below at parton level in a numerical integration.

### A. $gg \rightarrow g\gamma\gamma$

Consider first the process

$$g(p_1, \lambda_1, a) + g(p_2, \lambda_2, b) \rightarrow g(p_3, \lambda_3, c) + \gamma(p_4, \lambda_4) + \gamma(p_5, \lambda_5), \quad (3.11)$$

with the momenta  $p_i$  and the polarizations  $\lambda_i = \pm$  taken to be outgoing, and  $a, b, c$  are color adjoint labels. The corresponding matrix element can be written as a sum of continuum and resonant Higgs-mediated parts:

$$\mathcal{M} = \mathcal{M}^{\text{cont}} + \mathcal{M}^H. \quad (3.12)$$

For the Higgs-mediated contribution in Eq. (3.12), we will treat the gluon couplings to the Higgs using the effective theory in which the top quark is taken very heavy,  $M_t \gg M_H$ . Then one finds

$$\mathcal{M}_{\lambda_1\lambda_2\lambda_3\lambda_4\lambda_5}^H = \frac{g_3}{\sqrt{2}} f^{abc} C_g C_\gamma X_{\lambda_1\lambda_2\lambda_3} Y_{\lambda_4\lambda_5} / (h - M_H^2 + iM_H\Gamma_H), \quad (3.13)$$

with spinor-helicity factors:

$$\begin{aligned} X_{++++} &= -ih^2 / \langle 12 \rangle \langle 23 \rangle \langle 31 \rangle, \\ X_{----} &= ih^2 / [12][23][31], \end{aligned} \quad (3.14)$$

$$X_{+-+} = i[12]^3 / [23][31], \quad (3.15)$$

$$X_{--+} = -i\langle 12 \rangle^3 / \langle 23 \rangle \langle 31 \rangle,$$

$$X_{+--} = i[31]^3 / [12][23], \quad (3.16)$$

$$X_{-+-} = -i\langle 31 \rangle^3 / \langle 12 \rangle \langle 23 \rangle,$$

$$X_{-++} = i[23]^3 / [31][12], \quad (3.17)$$

$$X_{+--} = -i\langle 23 \rangle^3 / \langle 31 \rangle \langle 12 \rangle,$$

$$Y_{+++} = [45] / \langle 45 \rangle, \quad Y_{---} = \langle 45 \rangle / [45], \quad (3.18)$$

$$Y_{+-} = Y_{-+} = 0. \quad (3.19)$$

Note that these obey  $\langle ij \rangle \leftrightarrow [ji]$  when the helicities are flipped. The structure constants of the group are normalized so that  $f^{abc} f^{abd} = N\delta^{cd}$  with  $N = 3$  for QCD.

The continuum matrix element in Eq. (3.12) can be given in terms of the one-quark-loop 5-gluon partial amplitudes  $A_{5;1}^{[1/2]}$  that were obtained by Bern, Dixon, and Kosower in [57]. (These are somewhat complicated, and so will not be reproduced explicitly here. Note that flipping all of the helicities on  $A_{5;1}^{[1/2]}$  can be obtained by replacing  $\langle ij \rangle \leftrightarrow [ji]$  everywhere. In particular,  $\varepsilon(i, j, m, n) = [ij]\langle jm \rangle[mn] \times \langle ni \rangle - \langle ij \rangle[jm]\langle mn \rangle[ni]$  changes sign.) One finds, for massless quarks  $u, d, s, c, b$  circulating around the loop, and neglecting the suppressed top-quark contribution,

$$\mathcal{M}_{\lambda_1\lambda_2\lambda_3\lambda_4\lambda_5}^{\text{cont}} = \frac{g_3}{\sqrt{2}} f^{abc} \left( \frac{44}{9} \alpha_S \alpha \right) A_{\lambda_1\lambda_2\lambda_3\lambda_4\lambda_5}, \quad (3.20)$$

where [58,59]

$$\begin{aligned} A_{\lambda_1\lambda_2\lambda_3\lambda_4\lambda_5} &= 16\pi^2 [A_{5;1}^{[1/2]}(1, 2, 3, 4, 5) + A_{5;1}^{[1/2]}(1, 2, 3, 5, 4) + A_{5;1}^{[1/2]}(1, 2, 4, 3, 5) + A_{5;1}^{[1/2]}(1, 2, 5, 3, 4) \\ &\quad + A_{5;1}^{[1/2]}(1, 2, 4, 5, 3) + A_{5;1}^{[1/2]}(1, 2, 5, 4, 3) + A_{5;1}^{[1/2]}(1, 4, 2, 3, 5) + A_{5;1}^{[1/2]}(1, 4, 2, 5, 3) \\ &\quad + A_{5;1}^{[1/2]}(1, 4, 5, 2, 3) + A_{5;1}^{[1/2]}(1, 5, 2, 3, 4) + A_{5;1}^{[1/2]}(1, 5, 2, 4, 3) + A_{5;1}^{[1/2]}(1, 5, 4, 2, 3)]. \end{aligned} \quad (3.21)$$

The individual loop amplitudes  $A_{5;1}^{[1/2]}$  have infrared divergences, which cancel in the sum.

The spin and color sum/average for the reaction equation (3.11) is

$$\overline{\sum} \equiv \frac{1}{4} \sum_{\lambda_1, \lambda_2, \lambda_3, \lambda_4, \lambda_5} \frac{1}{(N^2 - 1)^2} \sum_{a, b, c}. \quad (3.22)$$

Taking into account  $Y_{+-} = Y_{-+} = 0$  and  $\langle ij \rangle [ij] = -s_{ij}$ , it follows that

$$\overline{\sum} |\mathcal{M}^H|^2 = \frac{3\pi\alpha_S}{4D(h)} |C_g C_\gamma|^2 \left( \frac{h^4 + \hat{s}^4 + s_{13}^4 + s_{23}^4}{\hat{s}s_{13}s_{23}} \right), \quad (3.23)$$

$$\begin{aligned} \overline{\sum} 2 \text{Re}[\mathcal{M}^H \mathcal{M}^{\text{cont}*}] &= \frac{11\pi\alpha_S^2\alpha}{12D(h)} \sum_{\lambda_1, \lambda_2, \lambda_3, \lambda_4} \{ (h - M_H^2) 2 \text{Re}[C_g C_\gamma X_{\lambda_1\lambda_2\lambda_3} Y_{\lambda_4\lambda_4} A_{\lambda_1\lambda_2\lambda_3\lambda_4\lambda_4}^*] \\ &\quad + M_H\Gamma_H 2 \text{Im}[C_g C_\gamma X_{\lambda_1\lambda_2\lambda_3} Y_{\lambda_4\lambda_4} A_{\lambda_1\lambda_2\lambda_3\lambda_4\lambda_4}^*] \}. \end{aligned} \quad (3.24)$$

In the following, we will neglect the small effects from  $\Gamma_H$ , so that, in Eq. (1.3), only Eq. (3.23) contributes to  $P(h)$  and only Eq. (3.24) contributes to  $I(h)$ . The pure continuum cross section has additional larger contributions from  $Q\bar{Q} \rightarrow \gamma\gamma$  and  $Qg \rightarrow Q\gamma\gamma$ , as well as from fake photons. Significant progress has been made on computing the diphoton backgrounds [60–64], but in experimental practice these are determined by fitting to sidebands; therefore the pure continuum is not considered here.

### B. $Q\bar{Q} \rightarrow g\gamma\gamma$

Next consider the process

$$Q(p_1, \lambda_1, j_1) + \bar{Q}(p_2, \lambda_2, j_2) \rightarrow g(p_3, \lambda_3, a) + \gamma(p_4, \lambda_4) + \gamma(p_5, \lambda_5), \quad (3.25)$$

where  $j_1, j_2$ , and  $a$  are  $SU(3)$  color indices in the antifundamental, fundamental, and adjoint representations. (The notation means that there is a quark in the initial state, with physical momentum and polarization  $-p_1$  and  $-\lambda_1$ , opposite to the outgoing momentum and polarization, and corresponding to an outgoing antiquark.) The Higgs-mediated contribution to this process has matrix element

$$\mathcal{M}^H = \frac{g_3}{\sqrt{2}} [\mathbf{t}^a]_{j_2}^{j_1} C_g C_\gamma Z_{\lambda_1 \lambda_2 \lambda_3} Y_{\lambda_4 \lambda_5} / (h - M_H^2 + iM_H \Gamma_H), \quad (3.26)$$

where  $C_g, C_\gamma$ , and  $Y_{\lambda_4 \lambda_5}$  are as given in Eqs. (2.5), (2.6), (3.18), and (3.19) above, and

$$Z_{-+-} = -\langle 13 \rangle^2 / \langle 12 \rangle, \quad Z_{+--} = [13]^2 / [12], \quad (3.27)$$

$$Z_{+--} = \langle 23 \rangle^2 / \langle 12 \rangle, \quad Z_{-++} = -[23]^2 / [12], \quad (3.28)$$

$$Z_{+++} = Z_{++-} = Z_{--+} = Z_{---} = 0, \quad (3.29)$$

and the generator matrices are normalized according to  $\text{Tr}[\mathbf{t}^a \mathbf{t}^b] = \delta^{ab}/2$ . For the continuum processes, the matrix elements can be written as

$$\mathcal{M}^{\text{cont}} = 8\sqrt{2}\pi e_Q^2 \alpha g_3 [\mathbf{t}^a]_{j_2}^{j_1} B_{\lambda_1 \lambda_2 \lambda_3 \lambda_4 \lambda_5}, \quad (3.30)$$

where  $e_Q = +2/3$  or  $-1/3$  is the charge of the quark  $Q = u, d, s, c, b$ . Because we are specifically interested in interference with diphotons from the Higgs boson, only the matrix elements with  $\lambda_4 = \lambda_5$  need to be considered. The continuum amplitude equation (3.30) vanishes if  $\lambda_3 = \lambda_4 = \lambda_5$ . So, there are only four helicity configurations that contribute to the interference. They are

$$B_{-++++} = \frac{\langle 12 \rangle \langle 13 \rangle^2}{\langle 14 \rangle \langle 15 \rangle \langle 24 \rangle \langle 25 \rangle}, \quad (3.31)$$

$$B_{+----} = -\frac{[12][13]^2}{[14][15][24][25]},$$

$$B_{+-----} = -\frac{\langle 12 \rangle \langle 23 \rangle^2}{\langle 14 \rangle \langle 15 \rangle \langle 24 \rangle \langle 25 \rangle}, \quad (3.32)$$

$$B_{-+---} = \frac{[12][23]^2}{[14][15][24][25]}.$$

The spin and color sum/average for the reaction equation (3.25) is

$$\bar{\sum} \equiv \frac{1}{4} \sum_{\lambda_1, \lambda_2, \lambda_3, \lambda_4, \lambda_5} \frac{1}{N^2} \sum_{j_i, j_2, a}. \quad (3.33)$$

It follows that

$$\bar{\sum} |\mathcal{M}^H|^2 = \frac{8\pi\alpha_S}{9D(h)} |C_g C_\gamma|^2 (s_{13}^2 + s_{23}^2) / s_{12}, \quad (3.34)$$

$$\bar{\sum} 2 \text{Re}[\mathcal{M}^H \mathcal{M}^{\text{cont}*}] = \frac{32\pi^2 e_Q^2 \alpha \alpha_S}{9D(h)} \sum_{\lambda_1 = \lambda_2, \lambda_3 = \lambda_4} \{ (h - M_H^2) 2 \text{Re}[C_g C_\gamma Z_{\lambda_1 \lambda_2 \lambda_3} Y_{\lambda_4 \lambda_4} B_{\lambda_1 \lambda_2 \lambda_3 \lambda_4 \lambda_4}^*] + M_H \Gamma_H 2 \text{Im}[C_g C_\gamma Z_{\lambda_1 \lambda_2 \lambda_3} Y_{\lambda_4 \lambda_4} B_{\lambda_1 \lambda_2 \lambda_3 \lambda_4 \lambda_4}^*] \}. \quad (3.35)$$

The contribution to  $pp \rightarrow j\gamma\gamma$  from  $Q\bar{Q} \rightarrow g\gamma\gamma$  involving the Higgs is numerically quite small, but is nevertheless included below. More importantly, it is useful because it is related by crossing to the processes of the next subsection.

### C. $Qg \rightarrow Q\gamma\gamma$ and $g\bar{Q} \rightarrow \bar{Q}\gamma\gamma$

Next consider the process

$$Q(p_1, \lambda_1, j_1) + g(p_2, \lambda_2, a) \rightarrow Q(p_3, \lambda_3, j_3) + \gamma(p_4, \lambda_4) + \gamma(p_5, \lambda_5). \quad (3.36)$$

The cross section can be obtained by crossing from the results of the previous section, by making the exchange

$2 \leftrightarrow 3$  in the spinor helicities  $\langle ij \rangle$  and  $[ij]$  and in  $s_{ij}$  in Eqs. (3.27), (3.28), (3.29), (3.31), (3.32), and (3.34), and by multiplying the right sides of Eqs. (3.34) and (3.35) by  $3/8$  to take into account

$$\bar{\sum} \equiv \frac{1}{4} \sum_{\lambda_1, \lambda_2, \lambda_3, \lambda_4, \lambda_5} \frac{1}{N(N^2 - 1)} \sum_{j_i, j_3, a}. \quad (3.37)$$

The cross section for  $g\bar{Q} \rightarrow \bar{Q}\gamma\gamma$  is obtained in the same way, except making instead the exchange  $1 \leftrightarrow 3$ ; it gives the same result after integrating over the final state angular variables.

#### IV. NUMERICAL RESULTS

This section contains numerical results for the shift in the diphoton mass distribution, as a function of the transverse momentum requirement on the final-state jet:

$$p_T^j > p_{T,\text{cut}}^j. \quad (4.1)$$

In the numerical integration, this and other cuts are imposed at parton level. Equation (4.1) is implemented simply by restricting the integrations over  $\hat{s}$  (or  $\tau$ ) and  $\chi$ , for fixed  $h$ , to the regions

$$\hat{s} > h + 2(p_{T,\text{cut}}^j)^2 \left[ 1 + \sqrt{1 + h/(p_{T,\text{cut}}^j)^2} \right], \quad (4.2)$$

$$|2\chi - 1| < \sqrt{1 - 4(p_{T,\text{cut}}^j)^2/[\hat{s}(1 - h/\hat{s})^2]}. \quad (4.3)$$

The other cuts are fixed and implemented within a Monte Carlo integration. The jet is required to be central:

$$|\eta_j| < 3.0. \quad (4.4)$$

For the photons, the cuts are

$$p_T^\gamma(\text{leading, subleading}) > (40, 30) \text{ GeV}, \quad (4.5)$$

$$|\eta_\gamma| < 2.5, \quad (4.6)$$

$$\Delta R_{\gamma\gamma}, \quad \Delta R_{j\gamma} > 0.4, \quad (4.7)$$

using the standard definition  $\Delta R = \sqrt{(\Delta\eta)^2 + (\Delta\phi)^2}$ . As in Sec. II, I use  $M_H = 125$  GeV and  $\Gamma_H = 4.2$  MeV, and MSTW 2008 NLO [54] parton distribution functions evaluated at  $\mu_F = M_H$ , with  $\alpha_S(\mu_R = 125 \text{ GeV}) = 0.114629$ , and other parameters listed there.

The cross sections for  $pp \rightarrow jH \rightarrow j\gamma\gamma$  and its parton-level constituents, as a function of the cut  $p_{T,\text{cut}}^j$ , are shown in Fig. 4 for  $pp$  collisions with  $\sqrt{s} = 8$  and 13 TeV. Also shown for comparison is the cross section for the leading order  $pp \rightarrow H \rightarrow \gamma\gamma$  with no jet requirement. The largest contribution is from  $gg \rightarrow gH \rightarrow g\gamma\gamma$ , especially for small  $p_{T,\text{cut}}^j$ . As expected, that parton-level cross section diverges as  $p_{T,\text{cut}}^j$  is taken to 0. The calculated  $pp \rightarrow jH \rightarrow j\gamma\gamma$  cross section exceeds that of the leading order tree-level cross section for  $pp \rightarrow H \rightarrow \gamma\gamma$ , with the same cuts on photons, when  $p_{T,\text{cut}}^j < 10$  GeV (at the 8 TeV LHC) or when  $p_{T,\text{cut}}^j < 12$  GeV (at the 13 TeV LHC). The calculation is only physically realistic for larger  $p_{T,\text{cut}}^j$ , e.g. 30 GeV as in [9,46–49]. The partonic processes  $Qg \rightarrow QH \rightarrow Q\gamma\gamma$  and  $\bar{Q}g \rightarrow \bar{Q}H \rightarrow \bar{Q}\gamma\gamma$  (combined in the figure) are subdominant, but certainly not negligible, while the process  $Q\bar{Q} \rightarrow gH \rightarrow g\gamma\gamma$  is an order of magnitude below the lower scale of the figure in each case.

A simple theoretical measure of the relative importance for  $\Delta M_{\gamma\gamma}$  of the interference compared to the pure resonance contribution, independent of the details of experimental mass resolution, is given by the dimensionless quantity

$$M_H \Gamma_H I(M_H^2)/P(M_H^2), \quad (4.8)$$

with  $I(h)$  and  $P(h)$  as defined in Eq. (1.3). Equation (4.8) is half of the ratio of the maximum deviation from 0 of the unsmeared interference line shape (which occurs at  $\sqrt{h} \approx M_H \pm \Gamma_H/2$ ) compared to the maximum of the pure resonant line shape (which occurs at  $\sqrt{h} = M_H$ ). The mass shift  $\Delta M_{\gamma\gamma}$  will be approximately proportional to Eq. (4.8), with a constant of proportionality that depends on mass resolution and other experimental realities including the

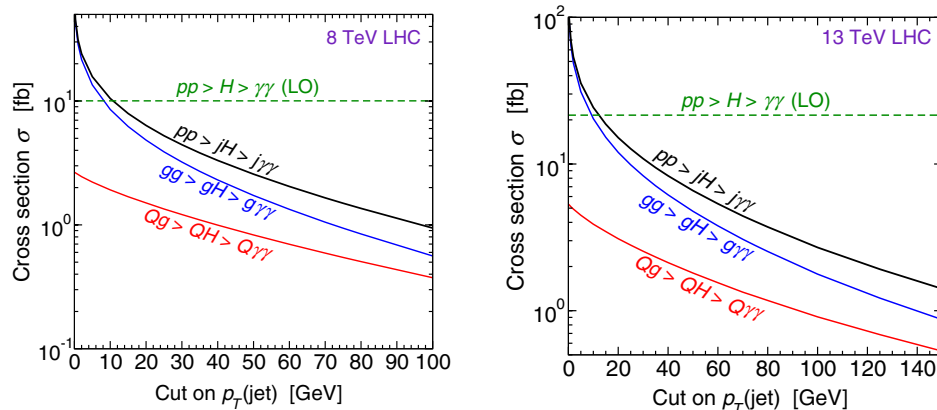


FIG. 4 (color online). Cross sections for  $pp \rightarrow jH \rightarrow j\gamma\gamma$ , as a function of the cut on the transverse momentum of the jet,  $p_{T,\text{cut}}^j$ , with other cuts and input parameters as described in the text. The portions coming from the  $gg$  and the  $Qg$  (plus  $\bar{Q}g$ ) parton level processes are shown separately; the  $Q\bar{Q}$ -initiated process is too small to show up on this scale. The cross section level for the leading order  $pp \rightarrow H \rightarrow \gamma\gamma$  with no jet requirement is also shown as the dashed line. The computation uses MSTW 2008 NLO parton distribution functions and  $\alpha_S$ , with  $\mu_R = \mu_F = M_H$ . The left panel is for  $pp$  collisions with  $\sqrt{s} = 8$  TeV, and the right panel for  $\sqrt{s} = 13$  TeV.

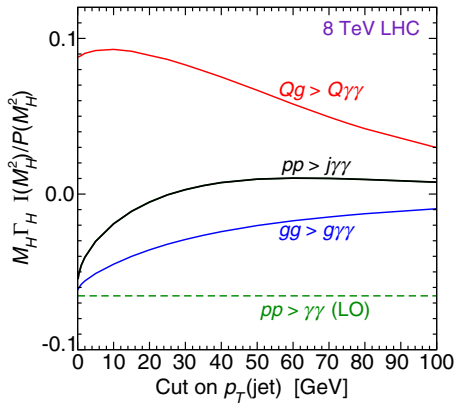


FIG. 5 (color online). The quantity  $M_H \Gamma_H I(M_H^2)/P(M_H^2)$ , where  $I(h)$  and  $P(h)$  are the functions defined in Eq. (1.3), as a function of the cut on the transverse momentum of the jet,  $p_{T,\text{cut}}^j$ , with other cuts as described in the text, for  $gg \rightarrow g\gamma\gamma$ , for  $Qg \rightarrow Q\gamma\gamma$  plus  $\bar{Q}g \rightarrow \bar{Q}\gamma\gamma$ , and for the combined  $pp \rightarrow j\gamma\gamma$ , for  $\sqrt{s} = 8$  TeV. The result for the leading order  $pp \rightarrow H \rightarrow \gamma\gamma$  with no jet requirement is also shown as the dashed line. The results for  $\sqrt{s} = 13$  TeV are similar.

method used to fit to the data. The value of this ratio is shown in Fig. 5 for  $gg \rightarrow g\gamma\gamma$ , and for  $Qg \rightarrow Q\gamma\gamma$  combined with  $\bar{Q}g \rightarrow \bar{Q}\gamma\gamma$ , and for the combined  $pp \rightarrow j\gamma\gamma$ , for  $\sqrt{s} = 8$  TeV. Note that as  $p_{T,\text{cut}}^j$  approaches 0 (the figure shows the computed values down to  $p_{T,\text{cut}}^j = 0.1$  GeV), the result for  $gg \rightarrow g\gamma\gamma$  is dominated by the log-enhanced contribution from diagrams with an extra gluon attached to the  $gg \rightarrow \gamma\gamma$  diagrams, and so the ratio approaches that for the leading order  $pp \rightarrow \gamma\gamma$ , which is also shown in the figure for comparison. For larger  $p_{T,\text{cut}}^j$ , the interference contribution for the  $gg \rightarrow g\gamma\gamma$  process maintains the same (negative) sign but becomes relatively smaller. Furthermore, as was already recently found in

Ref. [45], the sign of  $I(h)$  is positive for the  $Qg$ -initiated process. (The  $pp \rightarrow j\gamma\gamma$  curve is not the arithmetic sum of the  $gg \rightarrow g\gamma\gamma$  and  $Qg \rightarrow Q\gamma\gamma$  curves, because they have different weights in the combination.) Both of these effects contribute to the fact that the interference effect becomes much less important for finite  $p_{T,\text{cut}}^j$ , as compared to the leading order  $pp \rightarrow \gamma\gamma$  process with no jet, and it has the opposite sign for  $p_{T,\text{cut}}^j > 25$  GeV. The results shown are for  $\sqrt{s} = 8$  TeV; those for  $\sqrt{s} = 13$  TeV are quite similar.

The resulting shifts in the diphoton invariant mass peak,  $\Delta M_{\gamma\gamma} \equiv M_{\gamma\gamma}^{\text{peak}} - M_H$ , for both  $\sqrt{s} = 8$  and 13 TeV are shown in Fig. 6. These are computed as described in Sec. II, using representative Gaussian mass resolutions  $\sigma_{\text{MR}} = 1.3, 1.7, \text{ and } 2.1$  GeV. (Somewhat larger or smaller shift magnitudes could occur for different methods of fitting the line shape.) For any reasonable cut  $p_{T,\text{cut}}^j$ , the magnitude of the mass shift is much less than 100 MeV, and it is slightly positive for  $p_{T,\text{cut}}^j > 25$  GeV at the 8 TeV LHC and for  $p_{T,\text{cut}}^j > 36$  GeV at the 13 TeV LHC. This is in contrast to the negative shift of about  $(-95, -125, -155)$  MeV for  $\sigma_{\text{MR}} = (1.3, 1.7, 2.4)$  GeV from the leading order  $pp \rightarrow \gamma\gamma$  case with no jet as found in Sec. II and [30].

As in the leading order  $pp \rightarrow \gamma\gamma$  calculation of Sec. II, the choices of how to deal with parton distribution functions and  $\alpha_S$  and scale dependences on  $\mu_R$  and  $\mu_F$  have a big effect on the individual differential cross sections, but these tend to cancel out of the mass shift  $\Delta M_{\gamma\gamma}$ . In the case of  $gg \rightarrow g\gamma\gamma$ , both  $I(h)$  and  $P(h)$  are proportional to  $\alpha_S^3$ , so this common dependence leads to only a small effect on  $\Delta M_{\gamma\gamma}$  from choosing between NLO or LO  $\alpha_S$  or varying  $\mu_R$ . However, for the parton-level processes involving quarks, the function  $I(h)$  is proportional to  $\alpha_S^2$ , while  $P(h)$  is proportional to  $\alpha_S^3$ . This means that a choice of using the larger LO MSTW 2008  $\alpha_S(M_H)$  would yield a

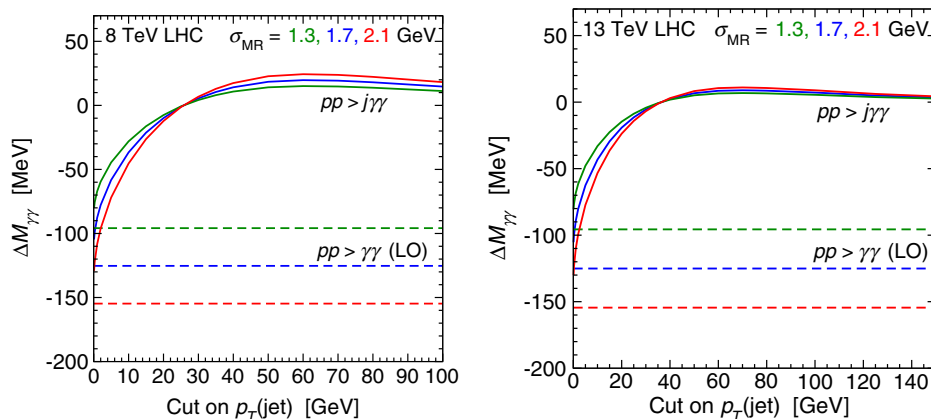


FIG. 6 (color online). The solid lines show the shifts in the diphoton mass peak,  $\Delta M_{\gamma\gamma} \equiv M_{\gamma\gamma}^{\text{peak}} - M_H$ , for  $pp \rightarrow j\gamma\gamma$ , as a function of the cut on the transverse momentum of the jet,  $p_{T,\text{cut}}^j$ , with other cuts as described in the text, for  $\sigma_{\text{MR}} = 1.3, 1.7, \text{ and } 2.1$  GeV (from top to bottom on the left). The dashed lines show the results for  $pp \rightarrow \gamma\gamma$  at leading order without a jet requirement, again for  $\sigma_{\text{MR}} = 1.3, 1.7, \text{ and } 2.1$  GeV (from top to bottom). The left panel is for  $pp$  collisions with  $\sqrt{s} = 8$  TeV, and the right panel for  $\sqrt{s} = 13$  TeV.

15% smaller contribution to the part of the shift that comes from  $Qg \rightarrow Q\gamma\gamma$ . A similar effect follows from any other renormalization scale choice that uses larger  $\alpha_S$  values. This will tend to shift the predicted value for the total  $\Delta M_{\gamma\gamma}$  down slightly from the curves shown in Fig. 6, without changing the conclusion that for reasonable values of  $p_{T,\text{cut}}^j$  the magnitude of the shift will be quite small.

## V. CONCLUSIONS

In this paper, I have evaluated the shift in the Higgs diphoton mass distribution for  $pp \rightarrow j\gamma\gamma$  due to interference between the resonant signal and continuum background. Unlike the result found in Ref. [30] at leading order for  $pp \rightarrow \gamma\gamma$  with no jet, the shift in the mass distribution is probably negligible, less than 20 MeV in magnitude for  $\sigma_{\text{MR}} = 1.7$  MeV, when the cut on the jet transverse momentum is large enough to be realistic. This is due in part to a reduction in the relative importance of the interference for  $gg \rightarrow g\gamma\gamma$  as compared to  $gg \rightarrow \gamma\gamma$ , and in part due to the opposite sign of the interference shift from the  $Qg \rightarrow Q\gamma\gamma$  process. The results for vector boson fusion  $pp \rightarrow jj\gamma\gamma$  and the 4-lepton  $pp \rightarrow ZZ^*$  final state

should both have very small interference effects. It is therefore tempting to speculate that if and when the Higgs diphoton mass measurement reaches the 100 MeV level of accuracy or better, the diphoton mass shift will be appreciable only for the exclusive  $pp \rightarrow \gamma\gamma$  channel with no additional jets passing cuts like the ones above, compared to the other classes of events contributing to the mass determination. However, from the results of Sec. IV, it appears that the difference between the diphoton mass peaks for events with no additional jets (corresponding to the leading order calculation) and those with a central jet with transverse momentum greater than 30 GeV might be as large as 150 MeV, for  $\sigma_{\text{MR}} = 1.7$  MeV. A full calculation including interference at NLO, at least, for the diphoton mass line shape would appear to be necessary to make a more definitive evaluation of this.

## ACKNOWLEDGMENTS

I am indebted to Daniel de Florian, Lance Dixon, and David Kosower for helpful discussions. This work was supported in part by the National Science Foundation Grant No. PHY-1068369.

- 
- [1] ATLAS Collaboration, *Phys. Lett. B* **716**, 1 (2012).
  - [2] CMS Collaboration, *Phys. Lett. B* **716**, 30 (2012).
  - [3] ATLAS Collaboration, Report No. ATLAS-CONF-2013-014, 2013.
  - [4] CMS Collaboration, Report No. CMS-PAS-HIG-12-045, 2012.
  - [5] H. M. Georgi, S. L. Glashow, M. E. Machacek, and D. V. Nanopoulos, *Phys. Rev. Lett.* **40**, 692 (1978).
  - [6] S. Dawson, *Nucl. Phys.* **B359**, 283 (1991).
  - [7] A. Djouadi, M. Spira, and P. M. Zerwas, *Phys. Lett. B* **264**, 440 (1991).
  - [8] M. Spira, A. Djouadi, D. Graudenz, and P. M. Zerwas, *Nucl. Phys.* **B453**, 17 (1995).
  - [9] D. de Florian, M. Grazzini, and Z. Kunszt, *Phys. Rev. Lett.* **82**, 5209 (1999).
  - [10] V. Ravindran, J. Smith, and W. L. Van Neerven, *Nucl. Phys.* **B634**, 247 (2002).
  - [11] C. J. Glosser and C. R. Schmidt, *J. High Energy Phys.* **12** (2002) 016.
  - [12] J. M. Campbell, R. K. Ellis, and G. Zanderighi, *J. High Energy Phys.* **10** (2006) 028.
  - [13] J. M. Campbell, R. K. Ellis, and C. Williams, *Phys. Rev. D* **81**, 074023 (2010).
  - [14] H. van Deurzen, N. Greiner, G. Luisoni, P. Mastrolia, E. Mirabella, G. Ossola, T. Peraro, J. F. von Soden-Fraunhofen, and F. Tramontano, *Phys. Lett. B* **721**, 74 (2013).
  - [15] R. V. Harlander and W. B. Kilgore, *Phys. Rev. Lett.* **88**, 201801 (2002).
  - [16] C. Anastasiou and K. Melnikov, *Nucl. Phys.* **B646**, 220 (2002).
  - [17] V. Ravindran, J. Smith, and W. L. van Neerven, *Nucl. Phys.* **B665**, 325 (2003).
  - [18] C. Anastasiou, K. Melnikov, and F. Petriello, *Nucl. Phys.* **B724**, 197 (2005).
  - [19] R. Boughezal, F. Caola, K. Melnikov, F. Petriello, and M. Schulze, *J. High Energy Phys.* **06** (2013) 072.
  - [20] U. Aglietti, R. Bonciani, G. Degrossi, and A. Vicini, *Phys. Lett. B* **595**, 432 (2004).
  - [21] S. Actis, G. Passarino, C. Sturm, and S. Uccirati, *Phys. Lett. B* **670**, 12 (2008).
  - [22] C. Anastasiou, R. Boughezal, and F. Petriello, *J. High Energy Phys.* **04** (2009) 003.
  - [23] S. Catani, D. de Florian, M. Grazzini, and P. Nason, *J. High Energy Phys.* **07** (2003) 028.
  - [24] G. Bozzi, S. Catani, D. de Florian, and M. Grazzini, *Nucl. Phys.* **B737**, 73 (2006).
  - [25] D. de Florian, G. Ferrera, M. Grazzini, and D. Tommasini, *J. High Energy Phys.* **11** (2011) 064.
  - [26] D. de Florian and M. Grazzini, *Phys. Lett. B* **674**, 291 (2009).
  - [27] S. Dittmaier *et al.* (LHC Higgs Cross Section Working Group Collaboration), [arXiv:1101.0593](https://arxiv.org/abs/1101.0593).
  - [28] S. Dittmaier *et al.*, [arXiv:1201.3084](https://arxiv.org/abs/1201.3084).
  - [29] C. Anastasiou, S. Buehler, F. Herzog, and A. Lazopoulos, *J. High Energy Phys.* **04** (2012) 004.
  - [30] S. P. Martin, *Phys. Rev. D* **86**, 073016 (2012).
  - [31] J. R. Ellis, M. K. Gaillard, and D. V. Nanopoulos, *Nucl. Phys.* **B106**, 292 (1976).

- [32] M. A. Shifman, A. I. Vainshtein, M. B. Voloshin, and V. I. Zakharov, *Yad. Fiz.* **30**, 1368 (1979) [*Sov. J. Nucl. Phys.* **30**, 711 (1979)].
- [33] J. F. Gunion, P. Kalyniak, M. Soldate, and P. Galison, *Phys. Rev. D* **34**, 101 (1986).
- [34] R. K. Ellis, I. Hinchliffe, M. Soldate, and J. J. van der Bij, *Nucl. Phys.* **B297**, 221 (1988).
- [35] J. F. Gunion, G. L. Kane, and J. Wudka, *Nucl. Phys.* **B299**, 231 (1988).
- [36] A. Djouadi, J. Kalinowski, and M. Spira, *Comput. Phys. Commun.* **108**, 56 (1998).
- [37] D. A. Dicus and S. S. D. Willenbrock, *Phys. Rev. D* **37**, 1801 (1988).
- [38] L. J. Dixon and M. S. Siu, *Phys. Rev. Lett.* **90**, 252001 (2003).
- [39] Z. Bern, A. De Freitas, and L. J. Dixon, *J. High Energy Phys.* **09** (2001) 037.
- [40] E. W. N. Glover and J. J. van der Bij, *Phys. Lett. B* **219**, 488 (1989); *Nucl. Phys.* **B321**, 561 (1989).
- [41] L. J. Dixon and Y. Sofianatos, *Phys. Rev. D* **79**, 033002 (2009).
- [42] J. M. Campbell, R. K. Ellis, and C. Williams, *J. High Energy Phys.* **10** (2011) 005.
- [43] G. Passarino, *J. High Energy Phys.* **08** (2012) 146.
- [44] N. Kauer and G. Passarino, *J. High Energy Phys.* **08** (2012) 116.
- [45] D. de Florian, N. Fianza, R. Hernández-Pinto, J. Mazzitelli, Y. Rotstein Habarnau, and G. Sborlini, *Eur. Phys. J. C* **73**, 2387 (2013).
- [46] S. Abdullin, M. Dubinin, V. Ilyin, D. Kovalenko, V. Savrin, and N. Stepanov, *Phys. Lett. B* **431**, 410 (1998).
- [47] V. V. Zmushko, Report No. ATL-PHYS-2002-020.
- [48] S. V. Demidov and D. S. Gorbunov, *Phys. At. Nucl.* **69**, 712 (2006).
- [49] O. Brein and W. Hollik, *Phys. Rev. D* **76**, 035002 (2007).
- [50] R. P. Kauffman, *Phys. Rev. D* **44**, 1415 (1991); S. Dawson and R. P. Kauffman, *Phys. Rev. Lett.* **68**, 2273 (1992); *Phys. Rev. D* **47**, 1264 (1993); **49**, 2298 (1994); R. P. Kauffman, S. V. Desai, and D. Risal, *Phys. Rev. D* **55**, 4005 (1997); **58**, 119901(E) (1998).
- [51] R. Karplus and M. Neuman, *Phys. Rev.* **83**, 776 (1951).
- [52] V. Costantini, B. De Tollis, and G. Pistoni, *Nuovo Cimento Soc. Ital. Fis. A* **2**, 733 (1971).
- [53] B. L. Combridge, *Nucl. Phys.* **B174**, 243 (1980).
- [54] A. D. Martin, W. J. Stirling, R. S. Thorne, and G. Watt, *Eur. Phys. J. C* **63**, 189 (2009).
- [55] M. L. Mangano and S. J. Parke, *Phys. Rep.* **200**, 301 (1991).
- [56] L. J. Dixon, [arXiv:hep-ph/9601359](https://arxiv.org/abs/hep-ph/9601359).
- [57] Z. Bern, L. J. Dixon, and D. A. Kosower, *Phys. Rev. Lett.* **70**, 2677 (1993).
- [58] D. de Florian and Z. Kunszt, *Phys. Lett. B* **460**, 184 (1999).
- [59] C. Balazs, P. M. Nadolsky, C. Schmidt, and C. P. Yuan, *Phys. Lett. B* **489**, 157 (2000).
- [60] T. Binoth, J. P. Guillet, E. Pilon, and M. Werlen, *Eur. Phys. J. C* **16**, 311 (2000); *Eur. Phys. J. direct C* **4**, 1 (2002).
- [61] Z. Bern, L. J. Dixon, and C. Schmidt, *Phys. Rev. D* **66**, 074018 (2002).
- [62] J. M. Campbell, R. K. Ellis, and C. Williams, *J. High Energy Phys.* **07** (2011) 018.
- [63] C. Balazs, E. L. Berger, P. M. Nadolsky, and C.-P. Yuan, *Phys. Lett. B* **637**, 235 (2006); P. M. Nadolsky, C. Balazs, E. L. Berger, and C.-P. Yuan, *Phys. Rev. D* **76**, 013008 (2007); C. Balazs, E. L. Berger, P. M. Nadolsky, and C.-P. Yuan, *Phys. Rev. D* **76**, 013009 (2007).
- [64] S. Catani, L. Cieri, D. de Florian, G. Ferrera, and M. Grazzini, *Phys. Rev. Lett.* **108**, 072001 (2012).